J. Water Environ. Nanotechnol., 5(1): 1-16 Winter 2020

ORIGINAL RESEARCH PAPER

Removing Methyl Orange Molecules from Aqueous Medium by Magnetic Nanoparticles: Evaluating adsorption factors, isotherms, kinetics and thermodynamics

Behgam Rahmanivahid[1], Fereshteh Naderi[2], Hamed Nayebzadeh[1,*]

[1] Department of Chemical Engineering, Esfarayen University of Technology, Esfarayen, North Khorasan, Iran
[2] Department of Chemistry, Shahr-e-Qods Branch, Islamic Azad University, Tehran, Iran

Received: 2019-10-31 Accepted: 2019-12-05 Published: 2020-02-01

ABSTRACT

In this paper, Fe_3O_4 and $MgFe_2O_4$ as magnetic samples were successfully synthesized by coprecipitation and combustion methods, respectively, to be used for adsorption of toxic methyl orange molecules from the aqueous solution. Characteristics of the synthesized samples were evaluated using various analyses. The results of crystalline and surface bonding assessment confirmed the successful synthesis of both samples with an appropriate structure. Moreover, Fe_3O_4 presented higher magnetic properties and surface area as well as lower pore diameter than $MgFe_2O_4$ sample. However, the maximum adsorption of methyl orange was obtained for $MgFe_2O_4$ (56.54 mg/g) which was around three times of Fe_3O_4 in the same conditions. This may be related to the larger pore diameter of $MgFe_2O_4$ and the ease of access to the internal surface of the adsorbent by the adsorbate molecules. Among the evaluated isotherms, the predicted Freundlich model showed a good correlation with the actual results of the adsorption process and the process could kinetically be explained by the pseudo-second-order equation. Thermodynamic investigation of the process showed the adsorption of methyl orange was exothermic and spontaneous. The results revealed that $MgFe_2O_4$ sample (q_{max} = 181.34 mg/g) can be suggested as a good adsorbent for the removal of toxic dyes and water pollutants.

Keywords: *Mg-Fe Spinel; Fe_3O_4; Magnetic Particles; Adsorption; Methyl Orange (MO).*

How to cite this article
Rahmanivahid B, Naderi F, Nayebzadeh H. Removing Methyl Orange Molecules from Aqueous Medium by Magnetic Nanoparticles: Evaluating adsorption factors, isotherms, kinetics and thermodynamics. J. Water Environ. Nanotechnol., 2020; 5(1): 1-16. DOI: 10.22090/jwent.2020.01.001

INTRODUCTION

Water as the most abundant constituent of the human body and the earth is one of the essential substances in the future of humans. Various pollutants such as heavy metals, biological, and dyes are brought into the water from various industries, which can have very devastating effects on human life and the environment. One of the most critical pollutants coming from different industries is waterborne dyes which are produced in industries such as the textile, clothing, dyeing, printing, and food industries [1,2]. These dyes contain toxic and carcinogenic substances that directly affect human health. The importance of these problems has led scientists in recent years to research the possible ways of removing colored substances from water. Chemical methods (dye decomposition), different membranes, and various adsorbents are the most important methods which had been proposed by researchers for removing dyes [3]. Among the methods mentioned, the use of dyes degradation [4] and adsorbents is more attractive for industrial applications due to their convenience and economy [5].

* Corresponding Author Email: h.nayebzadeh@esfarayen.ac.ir

The wide range of adsorbents has been employed in recent years with unique advantages and disadvantages [6]. In most of these studies, the practical factors on adsorption, the proposed isothermal model for the adsorption process (Langmuir, Freundlich, etc.), and the adsorption mechanism have been investigated [7]. For example, Khalil Ibrahim *et al.* used modified carbon nanotubes to remove methyl orange (MO) dye due to their high thermal and chemical stability [8]. Zayed *et al.* also used Egyptian Clays to remove MO from the aqueous solution [9]. Moreover, other materials such as silica nanoparticles [10] and zeolite/nickel ferrite/sodium alginate [11] as adsorbents had also been used for eliminating methylene blue dye.

Typical adsorbents used in the adsorption process (such as those mentioned above) have the same problem with difficulty in separation and filtration steps that will increase the cost of the process [12]. Therefore, the magnetic adsorbent can be one of the appropriate methods to overcome this problem to facilitate the adsorbent separation step [13]. Kukarni *et al.* studied the properties of Fe_3O_4 fabricated by two routes (co-precipitation and combustion method). They presented that the sample synthesized by the co-precipitation method represented better properties and magnetic activity [14]. In recent years, various mixed material magnetic absorbents such as activated carbon/$NiFe_2O_4$ [15], lignin-based nanoparticles [16], graphene/magnetite [17], magnetic carbon nanotubes [18], and magnetic carboxylated cellulose [19] have been evaluated in the literature. But, all of the above have complex synthesis steps or costly raw materials and synthesis methods.

Recently, spinels ($MgAl_2O_4$, $MgFe_2O_4$, $CuAl_2O_4$, etc.), which belong to the ceramics family, have been widely used in many industries due to their excellent properties such as chemical and thermal stability and mechanical strength [20]. Various methods for spinel synthesis have been reported in the literature; but, one of the simplest and least expensive ways in this regard is the combustion method [21]. $MgFe_2O_4$ were prepared by a facile solvothermal method after 2 days for removing of lead that the maximum adsorption capacity reached to 113.7 mg/g [22]. Lu *et al.* [23] studied the adsorption capacity of porous $MgFe_2O_4$/γ-Fe_2O_3 magnetic microspheres for the removals of dye (congo red). Although they presented high adsorption capacity for adsorbent, around 2 days consumed for the fabrication of $MgFe_2O_4$/γ-Fe_2O_3. $MgFe_2O_4$/biochar magnetic composites also utilized to remove phosphate from aqueous solutions in which the coprecipitation method was used for the preparation of adsorbent. Long and hard synthesis operation under specific conditions was done to obtain the sample after around 3 days [24]. $MgFe_2O_4$ modified by (Mn^{2+}, Co^{2+}, Ni^{2+}, and Cu^{2+}) has been used for adsorption of methylene blue which the maximum adsorption obtained at catalyst dose of 0.5 g/L and pH of 6.0. The glycine-nitrate method was used for the synthesis of $MgFe_2O_4$ which requires much time to obtain the proper adsorbent.

Considering the papers, in which magnetic spinels as adsorbents have been studied, showed that there are no reports of the use of the gel-combustion method in the synthesis of magnetic spinels. Instead of the combustion method, various synthesis methods such as coprecipitation, impregnation, sol-gel, etc. have been reported to synthesize spinels which require too much time and cost [25-27]. On the other hand, it is well known that the synthesis method could have a significant impact on changing spinel specifications [28-30]. However, a lack of study can detect on the spinel materials fabricated by solution combustion method. Moreover, comparing its properties and adsorption ability was not compared in any literature.

Accordingly, in this paper, the magnetic spinel $MgFe_2O_4$ was fabricated using a simple and inexpensive combustion method and its physicochemical properties, as well as its ability to be used as the adsorbent of MO, are compared with magnetic Fe_3O_4 synthesized by co-precipitation method. After choosing the best sample for reducing the concentration of MO from water, the useful parameters for the adsorption as the concentration of dye, adsorbent dosage, pH of the medium, and mixing rate (rpm) were then assessed and the proposed models for kinetics, isotherm, and thermodynamics of the adsorption process were precisely discussed.

MATERIALS AND METHODS

Nano Adsorbents Preparation and Procedure

For the synthesis of Fe_3O_4, iron (III) chloride nonahydrate and iron (II) sulfate heptahydrate with the molar ratio of 2 to 1 were stirred in a certain amount of deionized water under nitrogen atmosphere to give a uniform solution.

Subsequently, the NH_4OH aqueous (1.5 M) solution was added dropwise to precipitate the powder until the pH of the solution receives to 10. After ensuring complete deposition (a brown gel), the precipitate was separated by a magnet and washed several times with deionized water until the pH of the washed solution reached 7. Finally, the powder was dried at 50°C for 4 h to form the Fe_3O_4 adsorbent.

For synthesis $MgFe_2O_4$ adsorbent, iron (III) nitrate nonahydrate, and magnesium nitrate hexahydrate were first dissolved in a desirable amount of deionized water with the molar ratio of 0.5 Mg/Fe. Then, urea fuel was added to the solution at 1.5 times the stoichiometric ratio [21]. After 30 min of stirring on the hot plate at the ambient temperature, the solution temperature was brought to 70°C to form a brown gel by evaporating the water. Then, the brown viscose gel was placed in the oven at 350°C, and after a few minutes, the gel began to combust vigorously. Finally, $MgFe_2O_4$ brown powder was obtained.

Nano adsorbents Characterization Techniques

The Physico-chemical properties of the synthesized adsorbents were determined by X-Ray Diffraction (XRD), Field Emission Scanning Electron Microscopy (FESEM), Surface Particle Size Distribution (SPSD), Vibrating-Sample Magnetometer (VSM), Brunauer-Emmett-Teller (BET)/Barrett-Joyner-Halenda (BJH), Fourier Transform Infrared Spectroscopy (FTIR) and Thermogravimetry (TG) / Differential Thermal Analyser (DTA) analyses were used to investigate. An X'PertPro diffractometer (Holland, Panalytical, Cu Kα: 1.54 angstrom) was used to evaluate the crystalline phases and structure of the samples in the range of 10–80°. The crystalline size of the samples was measured by Scherer's equation as shown below:

$$D= 0.9\lambda/\beta.Cos\theta$$

Where D, λ, β, and θ are crystalline sizes (nm), radiation wavelength (1.5406 Å), corrected half-width of the peak profile and corrected half-width of the diffraction peak angle, respectively.

A MIRA3 FE-SEM device (Czech Republic, TESCAN) was used to assess the surface morphology of the adsorbents. ImageJ software was also used to examine the SPSD of samples. The VSM analysis, which obtained from an MDKB analyzer (Iran, Magnetic Daghigh Kavir), was used to investigate the magnetic strength of the adsorbents. BET-BJH analysis was obtained from a Belsorp mini II analyzer (Japan, Microtrac Bel Corp.). This analysis was used to determine the surface area, pore diameter, and volume of synthesized adsorbents (The degassing of samples was done at 220 °C for 3 h). The Spectrum Two analyzer (USA, Perkin Elmer) was used to take FTIR analysis in the 400-4000 cm^{-1} range using the K-Br tablet method to detection of functional groups belonged to magnetic adsorbents and remained precursors. The TGA also performed by an STA503 instrument (Germany, BAHR) in the range of 30°C to 800°C with a 10°C/min increasing rate and by an argon flow (70 cm^3/min).

Experimental Setup for Adsorption Performance Test

The methyl orange solution (aq.) was used to investigate the activity of the synthesized adsorbents. For this purpose, the aqueous solution of methyl orange was used at different concentrations (described in the adsorbents efficiency section). In each experiment, specific amounts of adsorbent were added to 50 ml of methyl orange solution to perform the adsorption process. Then, the solution was placed on a shaker to disperse the adsorbent in the methyl orange solution. After the adsorption process was completed, the adsorbent was separated from the solution by a magnet and, then, the centrifuge was used to ensure the complete removal of non-visible absorbent nanoparticles. Finally, UV analysis was used to obtain the amount of methyl orange absorption. A calibration curve of Methyl Orange concentration versus UV absorbance was used to calculate the MO concentration. This curve was prepared by measuring the UV absorbance at 464 nm in an MO concentration region of 5-120 mg/L (Fig. S1). UV analysis was performed by UV-2600 spectrophotometer (Japan, Shimadzu) and each water sample was evaluated three times to ensure the accuracy of the results of each experiment.

RESULTS AND DISCUSSIONS

Assessment the properties of Nano Adsorbents

XRD Analysis

The XRD analysis of the synthesized adsorbents and the standard pattern of the related materials are given in Fig. 1(a). The figure shows that the peaks created for the Fe_3O_4 sample were in perfect agreement with the standard pattern (Cubic, pattern

ICDD -01-075-0033). Comparing the sample peaks with the standard pattern of Fe_2O_3 (Rhombohedral, pattern ICDD -01-084-0306) revealed that no Fe_2O_3 was synthesized during the synthesis of the Fe_3O_4 sample. By simultaneously evaluating the sample peaks of $MgFe_2O_4$ and the reference pattern of $MgFe_2O_4$ (Cubic, pattern ICDD-01-073-2211), it can be concluded that the magnetic spinel of $MgFe_2O_4$ was correctly synthesized. It observes that the positions of Fe_3O_4 and $MgFe_2O_4$ are the same. It must be mentioned that Fe_3O_4 and $MgFe_2O_4$ have a spinel structure in which the structure was changed from inverse spinal (Fe_3O_4) to spinel structure ($MgFe_2O_4$) by doping Mg cations [31]. Fe_3O_4 presents the inverse spinel structure in which Fe^{+2} ions occupy the octahedral (B) sites and Fe^{+3} ions occupy both the tetrahedral (A) and octahedral sites ($[Fe^{+3}]_A[Fe^{+3}Fe^{+2}]_BO_4$) [19, 35] equally. The inversion parameter decreased with the diffusion of Mg into Fe_3O_4 lattice. Therefore shifting in the peak positions can detect [32]. Moreover, replacing the Fe cations with Mg cation can affect the positions of peaks due to the difference in the atomic radius of Mg and Fe cations [33].

The MgO (Cubic, ICDD-01-077-2364) was also illustrated in the figure to ensure the synthesis of $MgFe_2O_4$ due to the similarity of the standard pattern of the Fe_3O_4 and $MgFe_2O_4$ to each other. It must be mentioned that if the spinel structure was not synthesized, the peak of MgO should be observed in the XRD pattern. The size of the synthesized adsorbent crystals (calculated using the Scherrer equation [34]) is shown in Table 1. The crystalline size of Fe_3O_4 and $MgFe_2O_4$ samples were obtained as 11.9 nm and 7 nm, respectively, indicating that both adsorbents belonged to the nanomaterial family.

FTIR Analysis

The FTIR analysis was taken from both samples to investigate the functional groups and their bond type, as shown in Fig. 1(b). Two significant peaks created at 3410 and 1615 cm^{-1} were related to the O-H stretching-bending bonds of the adsorbed water molecules on the surface samples [35]. The peaks at 2830 and 2910 cm^{-1} for $MgFe_2O_4$ represented the C-H (stretching-vibration) bonds of urea fuel, which was used in the synthesis process [21]. The presence of these peaks indicated that the fuel did not completely consume during the synthesis process; but, nothing can be said about its value. A large peak created for the $MgFe_2O_4$ sample at 1060 cm^{-1} was related to C-N group bonds in urea fuel [36] and, on the other hand, peaks formed at 900, 1390 and 1615 cm^{-1} in the same sample were related to the vibration bonds of NO^{3-} group. These peaks indicated the presence of some nitrate in the adsorbents (remaining from the synthesis steps,

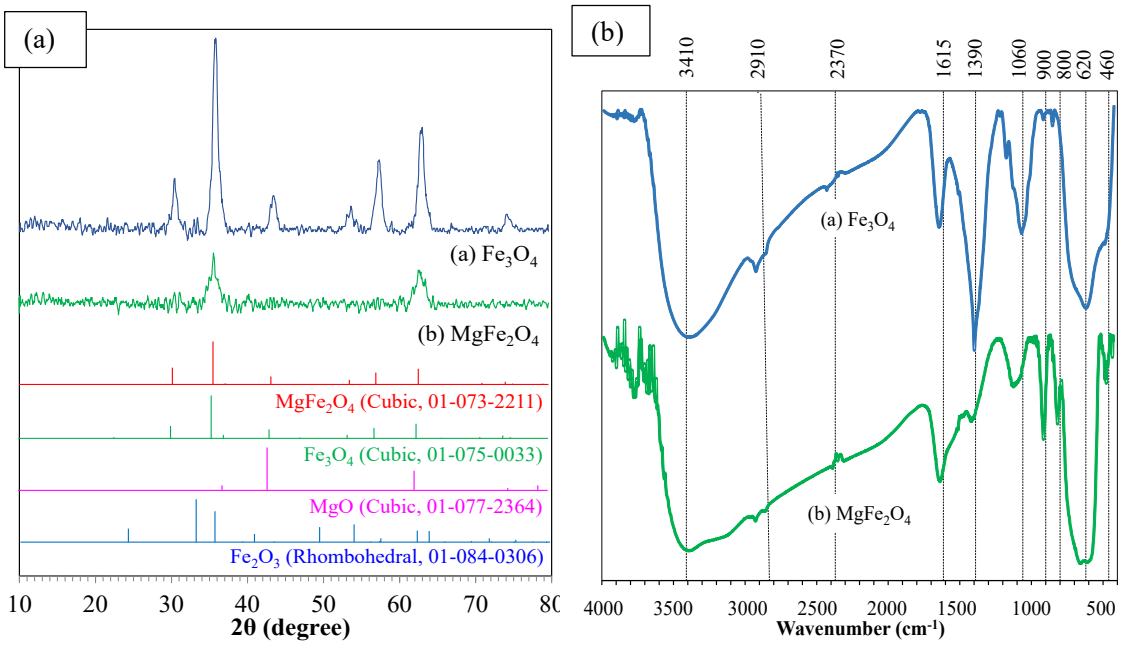

Fig. 1. XRD patterns of Fe_3O_4 and $MgFe_2O_4$ nano adsorbents: (a) Fe_3O_4, (b) $MgFe_2O_4$.

Table 1. Structural properties of Fe_3O_4 and $MgFe_2O_4$ nano adsorbents.

Nano adsorbent	Synthesis Method	S_{BET} (m^2/g)	V_p (cm^3/g)	D_p (nm)	Crystallite size[a] (nm)
Fe_3O_4	Precipitation	80.3	0.375	5.4	11.9[b]
$MgFe_2O_4$	Combustion	52.1	0.216	6.9	7[c]

a. Crystallite size estimated by Scherrer's equation.
b. Crystallite phase: Cubic (JCPDS: 01-077-2364, 2θ = 18.3°, 30.1°, 35.5°, 37.1°, 43.1°, 53.5°, 57.0°, 62.6°, 74.1°, 89.8°)
c. Crystallite phase: Cubic (JCPDS: 01-073-1960, 2θ = 30.2°, 35.6°, 43.2°, 53.6°, 57.2°, 62.8°, 74.3°)

which could be determined by TG analysis) [37]. The presence of peaks of 1060 and 1390 cm^{-1} in the Fe_3O_4 sample was related to the S = O group of residual precursors remained from the synthesis process of this sample [38]. Finally, with peaks in the range of 400 to 900 cm^{-1}, the synthesis of Fe_3O_4 and $MgFe_2O_4$ adsorbents can be assured. It can observe that only one peak at 460 cm^{-1} appears for Fe_3O_4, which could be related to Fe-O bonding while two peaks detected in 440 cm^{-1} and 460 cm^{-1} related to Mg-O and Fe-O for $MgFe_2O_4$, respectively [39,37].

FESEM Analysis

The FESEM analysis of both synthesized samples was performed, the results of which are visible in Fig. 2. The study of both adsorbents revealed that the samples had nano-dimensions. Both Fe_3O_4 and $MgFe_2O_4$ seemed to have the

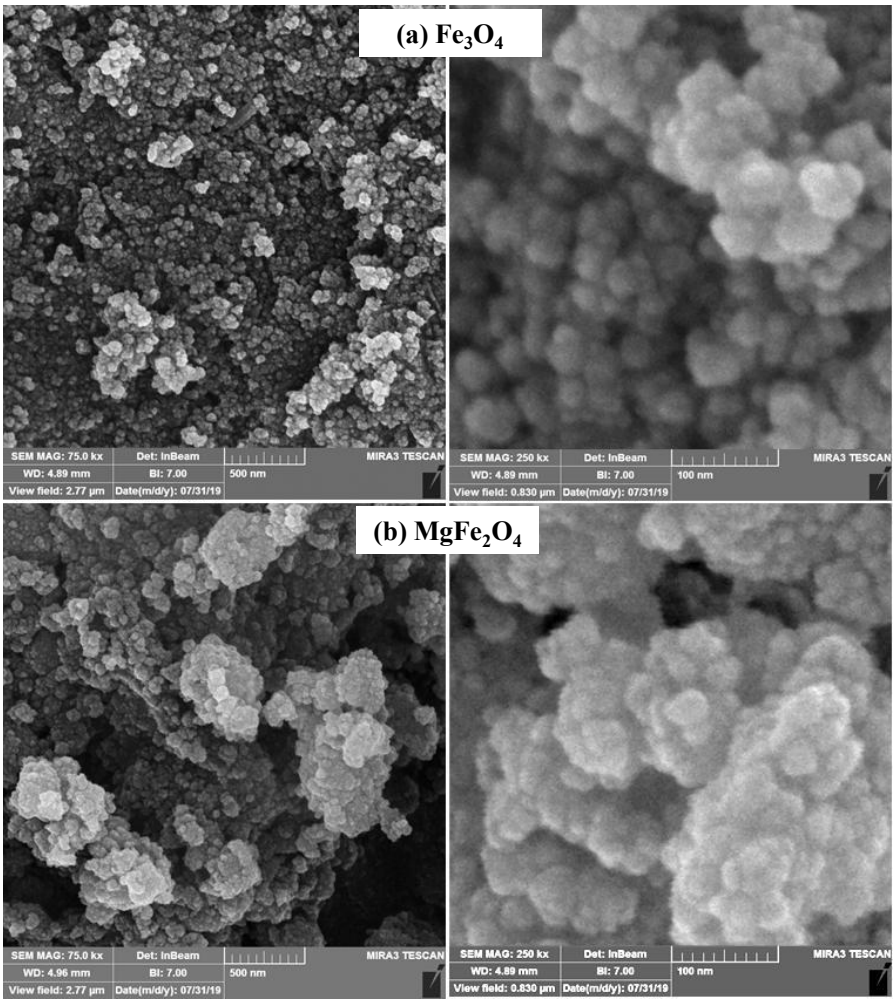

Fig. 2. FESEM images of Fe_3O_4 and $MgFe_2O_4$ nano adsorbents: (a) Fe_3O_4, (b) $MgFe_2O_4$.

same morphology; however, more uniformity was detected in the structure of the Fe_3O_4 adsorbent. The uniformity could be due to the differences in the synthesis procedures. The sample synthesized by the combustion method due to the uncontrollable nature of the combustion process had more agglomerated particles than the sample synthesized by the co-precipitation method. On the other hand, the use of the combustion method resulted in the formation of more cavities in the $MgFe_2O_4$ spinel, which might be due to the combustion gases removed from the original gel composition [40]. More porosity with a larger pore diameter caused by the combustion synthesis method can have a noteworthy effect on the absorption of large molecules (such as methyl orange). It makes more accessible the internal surface area of the materials (inside the pores) to dye molecules for easier diffusion/permission [41].

To further investigate the effect of the combustion synthesis method (the $MgFe_2O_4$ adsorbent was further investigated because of its much better performance in the adsorption process), the FESEM images of $MgFe_2O_4$ spinel were evaluated using ImageJ software [37] to obtain surface particle size distribution (SPSD). Results of this evaluation, which are mentioned in Fig. 3, showed that the largest and lowest particle sizes in spinel adsorbent were 25.9 and 5.6 nm, respectively, and the average particle size was 14.5 nm. The SPSD also exhibits that the particle size distribution is pointedly in the 10-20 nm range, which was significant for a nano-adsorbent.

VSM Analysis

Magnetic properties of the synthesized samples are one of their important characteristics to provide a simple separation condition after the adsorption of the dyes. For this purpose, VSM analysis was applied as shown in Fig. 4. The saturation magnetic strength for the Fe_3O_4 and $MgFe_2O_4$ was 48.79 emu/g and 1.79 emu/g, respectively. Due to the presence of Mg in the structure of $MgFe_2O_4$, decreasing in magnetic strength was predictable. Reduction in the saturation magnetization can be also assigned to the annealing process (combustion process) that it renders domains motion/rotation and leads to higher kinetic energy [42,43].

It is also clear that there was no hysteresis for both samples which is related to a superpara-

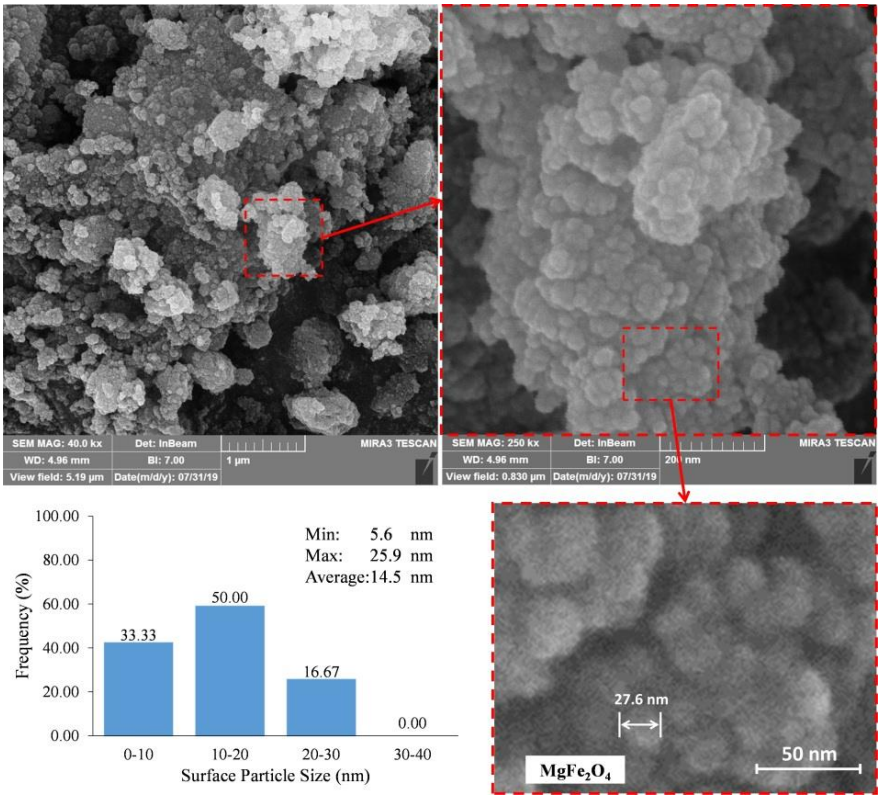

Fig. 3. Surface Particle size distribution histogram of $MgFe_2O_4$ nano adsorbents.

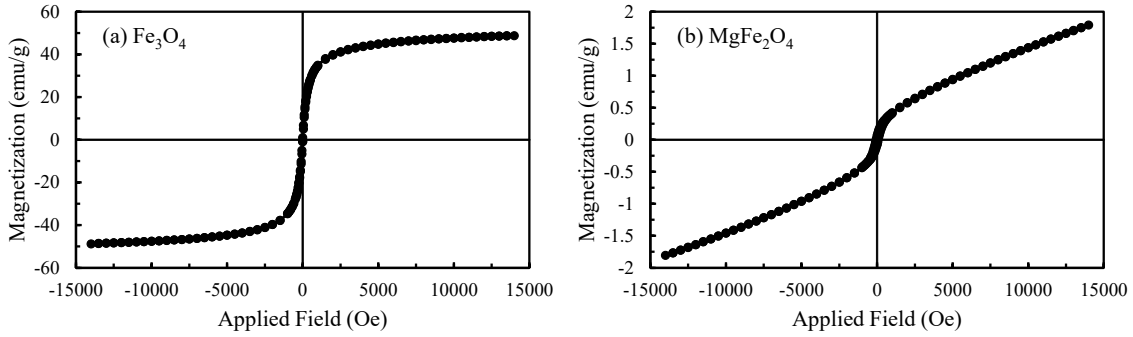

Fig. 4. VSM analyses of Fe_3O_4 and $MgFe_2O_4$ nano adsorbents: (a) Fe_3O_4, (b) $MgFe_2O_4$.

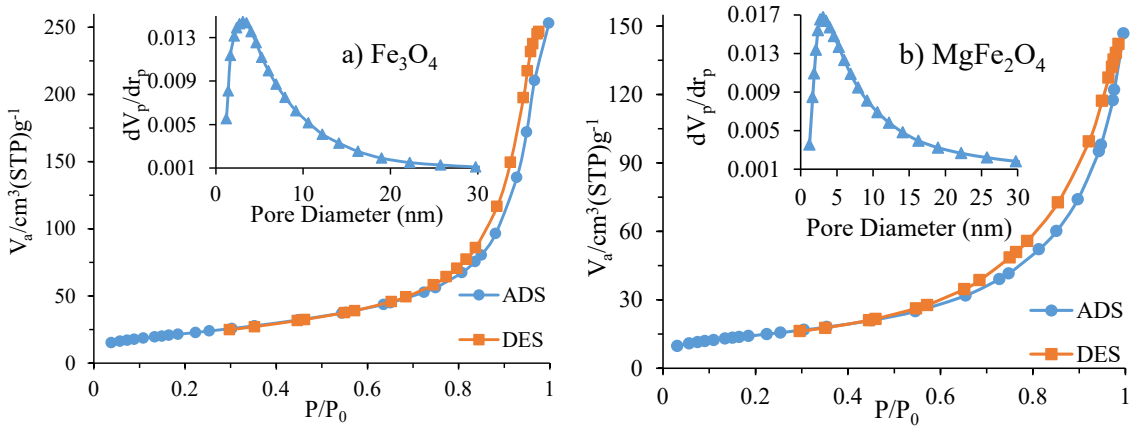

Fig. 5. Adsorption/Desorption isotherms and pore size distribution of Fe_3O_4 and $MgFe_2O_4$ nano adsorbents: (a) Fe_3O_4, (b) $MgFe_2O_4$.

magnetic nature [35]. These materials do not cling to each other (agglomeration) in the absence of a magnetic field because they only have the magnetic properties in the presence of the field, making them easy to use as adsorbents [44].

BET/BJH Analysis

One of the most important parameters in the adsorption process is the surface area and pore volume and diameter of the adsorbent. These specifications were obtained for both studied samples by BET-BJH analysis, the results of which are presented in Table 1 and Fig. 5. It can be observed in Table 1 that the specific surface area of Fe_3O_4 was about 1.5 times of the magnetic spinel of $MgFe_2O_4$. The difference in surface area can be due to the different nature of the two materials as well as the various synthesis methods [21]. Also, by comparing the pore volume and diameters, it is found that the Fe_3O_4 adsorbent had higher pore volume, but lower pore diameter than the magnetic spinel. Due to the large size of the methyl orange molecules, the used adsorbent must have a large pore diameter to allow a better adsorption process. Therefore, the $MgFe_2O_4$ sample with an average pore diameter of 6.9 nm compared to Fe_3O_4 with the average pore diameter of 5.4 nm can be better adsorbent for coarse methyl orange molecules [45]. It can be observed that both adsorbents fell into category IV of the IUPAC classification for porous materials (that were related to mesopore materials) by examining Fig. 5 and the absorption curves of the two synthesized magnetic samples. The adsorption-desorption hysteresis of both adsorbents was also very similar to the H1 type, which indicated the formation of cylindrical holes in the adsorbents. The created cylindrical pores in the samples can facilitate the entry of large methyl orange molecules into the adsorbent pores and, thus, increase access to the internal adsorbent surface [34]. As seen in Fig. 5, the maximum size distribution of the pore diameters of both adsorbents was in the range of 2

to 30 nm, which proved that the adsorbents were mesopore (2–50 nm).

TG Analysis

TG analysis was used to qualitatively evaluate the synthesized adsorbents, the results of which are shown in Fig. 6. The amount of additional material (such as water, precursors, etc.) remained in/on the samples can be evaluated using this analysis. The Fe_3O_4 and $MgFe_2O_4$ samples showed a 3 and 12% decrease in weight between 30-200°C, respectively. This reduction might be due to the absorption of gases in the atmosphere, such as water and carbon dioxide, onto the surface of the adsorbents. There was also a 3.3% decrease in Fe_3O_4 sample at the temperatures between 200 and 450°C, which could be related to the decomposition of chloride and sulfate compounds in the precursors. In the same temperature range for the $MgFe_2O_4$ magnetic spinel, a 12% decrease in weight was observed, which was due to the decomposition of the nitrate precursor materials used in the synthesis of this sample. Finally, at temperatures above 450°C, almost no decrease was observed in the Fe_3O_4 sample; but, for the $MgFe_2O_4$ spinel, a decrease of about 5.3% was achieved, which could be due to the decomposition of urea fuel remaining from the combustion stage in this sample. According to the results, there was a good agreement between the results of FTIR and TG analysis.

Performance Study toward Removal of Methyl Orange

Optimum adsorbent

Both synthesized adsorbents were investigated under similar conditions in the methyl orange adsorption process from water. For this purpose, 0.05 g of the adsorbent was poured into 50 ml of

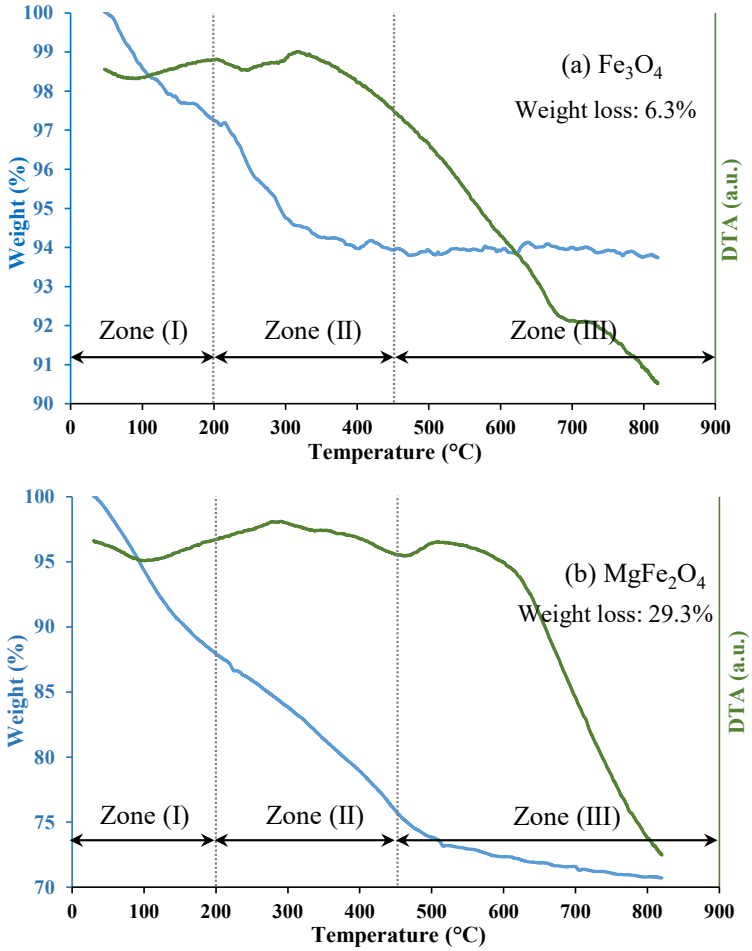

Fig. 6. TG Analyses of Fe_3O_4 and $MgFe_2O_4$ nano adsorbents: (a) Fe_3O_4, (b) $MgFe_2O_4$.

methyl orange solution in water (100 mg MO/L) at pH 6. The solution with the adsorbent was placed in a shaker at 200 rpm and the mixing temperature was adjusted to 25°C. After 1 h of the adsorption process, some samples were taken from both test vessels by a syringe containing a filter syringe. To ensure that no adsorbent was present in the sample solution, they were centrifuged at 6000 rpm for 15 min. Then, spectrophotometer analysis in the range of 350 to 600 cm^{-1} was used to obtain methyl orange absorption.

The results showed that the adsorption amount of MO on the surface of Fe_3O_4 and $MgFe_2O_4$ adsorbents in the mentioned condition was 20 mg/g and 56.54 mg/g, respectively. Thus, it was found that the $MgFe_2O_4$ sample had stronger adsorption on methyl orange. Therefore, following the optimum process conditions, isotherms, thermodynamics, and kinetics of adsorption of this sample will be examined in the next sections.

Adsorption Optimum Conditions

The effective factors of pH, adsorbent amount, contact time, stirring rate, and temperature for evaluating the best adsorption conditions were investigated. The factors were assessed based on the one-factor-at-a-time method, meaning that the values of a factor were changed while the other factors were fixed. Fig. 7 shows diagrams of factors affecting the adsorption process. As shown in Fig. 7a, by increasing the pH from 2 to 10 (methyl orange concentration = 100 mg/L, stirring speed = 200 rpm, contact time = 15 min and adsorbent dosage = 1 g/L), the adsorption amount was initially increased until pH 6 and, then, decreased. It can be referred to as surface change or ionization of methyl orange molecules, in which the adsorbent surface had the highest amount of positive charge at pH = 6 for higher adsorption of methyl orange anion molecules [8]. By increasing the pH of the solution, in addition to reducing the positive surface charges of the adsorbent, the negative ions from the alkaline solution also increase. As these negative ions increase, the competition for adsorption on the adsorbent increases. In other words, MO anion molecules and alkaline-negative ions compete for adsorption on the adsorbent surface with a positive

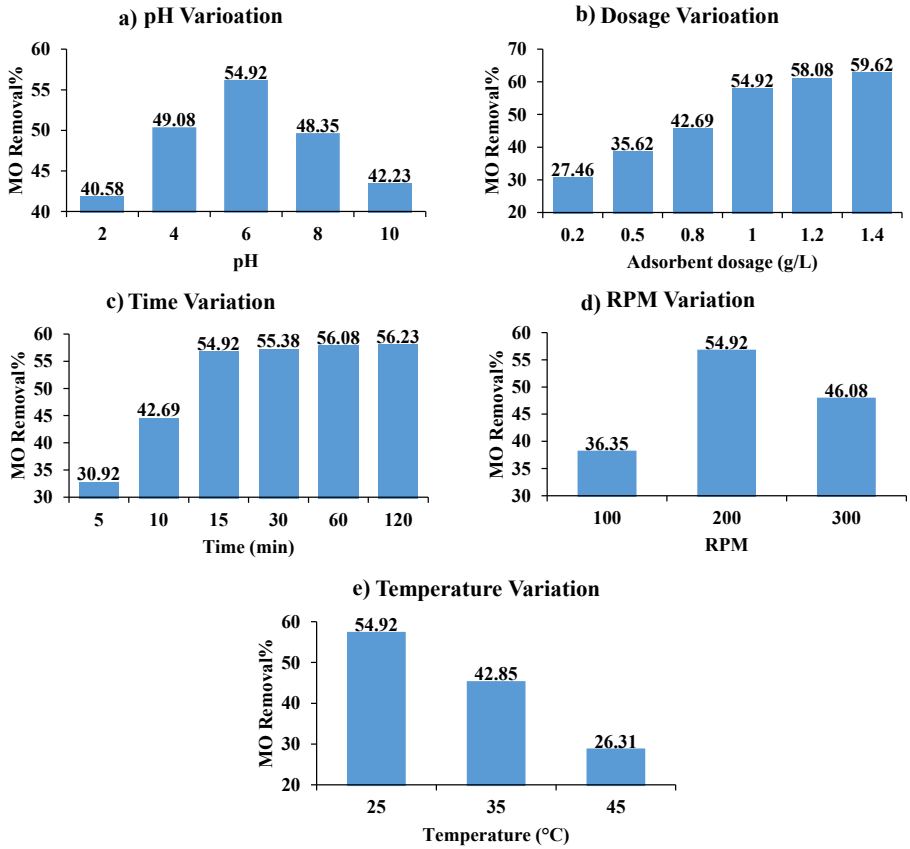

Fig. 7. Effect of adsorption condition variation on adsorption performance of $MgFe_2O_4$

charge [46]. Other articles have reported the same phenomena that methyl orange adsorption is observed in almost neutral pH [47]. From the results, it can be said that the interaction between the adsorbent and adsorbate molecules is the type of electrostatic forces [48].

The effect of increasing the adsorbent (Fig. 7b) more than 1 g/L showed that the adsorption amount did not increase significantly, which could be due to the interaction of the adsorbent particles with each other and disruption of the proper distribution as well as the increment viscosity of the solution by increasing amount of solid phase [47,3]. In some articles, it has been reported that the amount of adsorption decreases with the increasing amount of adsorbent due to changes in the viscosity of the solution or the limitation of the presence of adsorbate molecules around the adsorbent. [49,50].

The same behavior was observed by increasing the contact time, whereby the adsorption increased to reach equilibrium after about 15 min (Fig. 7c). Due to the saturation of the adsorbent surface with the dye and limitation in mass transfer, the equilibrium would be established and the adsorption value did not change appreciably.

Fig. 7d and Fig. 7e show the effect of changing stirring speed and temperature, respectively. Accordingly, the highest absorption was observed at 200 rpm. It seems that mixing was not performed well at 100 rpm. Also adsorbent did not disperse properly in the solution due to the absorption vortex at 300 rpm. In other words, by creating a vortex, the fluid will move like a rigid object, and as a result, the adsorbent will not mix properly with the adsorbate in the solution [51]. Examination of temperature change showed that, as the temperature increased, the amount of adsorption decreased, indicating that the adsorption was an exothermic process. According to the studies, the maximum adsorption of methyl orange on $MgFe_2O_4$ magnetic adsorbent was obtained at pH = 6, adsorbent content of 1 g/L, the contact time of 15 min, stirring speed of 200 rpm, and temperature of 25°C. Other essential aspects of the adsorption process were investigated under these conditions.

Isotherms

One of the important points in the adsorption process is the investigation of adsorption isotherms, which allows for investigating the type of interaction between the adsorbent and the adsorbate as well as the final adsorbent capacity. For this purpose, four important isotherms of Langmuir, Freundlich, Temkin, and Dubinin–Radushkevich were investigated for the methyl orange adsorption process on $MgFe_2O_4$ surface. The linear equations of these isotherms were evaluated, the results of which are shown in Table 2 and Fig. S2. Fig. S2(a) shows that, at low concentrations of methyl orange (up to 100 mg/L), there was a good agreement between the adsorption data and the Langmuir model (R^2 = 0.984 and maximum

Table 2. Linearized equations of isotherm models for the adsorption of MO on the $MgFe_2O_4$ surface.

Isotherm Models	Linearized equations	Parameters	
Langmuir	$\frac{C_e}{q_e}=\frac{1}{K_L q_m}+\left(\frac{1}{q_m}\right)C_e$	R^2	0.8415
		q_m (mg/g)	108.69
		K_L (L/mg)	0.019
Freundlich	$\ln q_e = \ln K_F + \frac{1}{n}\ln C_e$	R^2	0.949
		n	1.33
		K_F (mg/g)	2.928
		q_m (mg/g)	181.34
Temkin	$q_e = B_1 \ln k_t + B_1 \ln C_e$	R^2	0.9485
		B_1	22.417
		k_t (L/mg)	0.212
Dubinin - Radushkevich	$\ln q_e = \ln q_m - K_D \varepsilon^2$	R^2	0.8727
		q_m (mg/g)	47.87
		K_D	0.0003
		E (J/mol)=1/(2K_D)$^{0.5}$	29

q_m: the maximum adsorption capacity, K_L: Langmuir equilibrium constant, K_F & n: Freundlich equation constants, k_t: the equilibrium binding constant, B_1: the heat of adsorption, K_D: the activity coefficient constant related to adsorption energy, ε^2: Polanyi potential, E: the mean free energy of adsorption.

adsorption capacity = 243.9 mg/g), but with an increase in the initial concentration of adsorbate, the regression coefficient was reduced to 0.8415. The maximum capacity using the Langmuir model obtains 108.7 mg/g (Table 2). The Langmuir isotherm expressed monolayer adsorption on the homogeneous adsorbent surface. So, by coating a layer of adsorbate on the adsorbent surface, the adsorption process reached its maximum value [3].

The high accuracy between adsorption data with the Freundlich model, which expressed the multilayer adsorption of adsorbate on the heterogeneous adsorbent surface [8], can confirm the results (Table 2, Fig. S2b). The results showed that the adsorption process followed the Freundlich theory (R^2 = 0.949) in the range of low to high concentrations of methyl orange. The slope of the line (1/n = 0.75) in the Freundlich equation expressed the adsorption power of the dye on the heterogeneous adsorbent and its smaller values (0 < 1/n < 1) indicated more similarity of the adsorption process to the heterogeneous system and confirmed the suitability of the adsorbent [52]. The maximum adsorption capacity (q_m) for the Freundlich model can be calculated from the $q_m=K_F C_0^{1/n}$ formula, in which the initial concentration of MO (C_0) is constant against the amount of adsorbent (K_F & n = Freundlich equation constants) [53]. q_m was obtained 181.34 mg/g that revealed Mg-Fe spinel ($MgFe_2O_4$) can be an appropriate adsorbent for the dye adsorption process.

Temkin model was also studied on the adsorption data, as presented in Table 2 and Fig. S2c. This theory also evaluates the interaction between the adsorbate (methyl orange) and the adsorbent ($MgFe_2O_4$) as well as its relationship to bond energy. The results demonstrated that the adsorption data were in good agreement with this isotherm model (R^2 = 0.948). High consistency of the adsorption data with Temkin theory indicated a strong interaction between the adsorbate and the adsorbent [54].

The last studied isotherm, shown in Table 2 and Fig. S2d, was the Dubinin–Radushkevich model, in which the type of adsorption (chemically or physically), as well as the adsorption mechanism on the surface of heterogeneous porous adsorbents, was presented [55]. As shown in the figure, there was a great deal of agreement between the linearized isotherm equation and the adsorption data (R^2 = 0.964) at high concentrations, while less compatibility was observed at low adsorbate concentrations (R^2 = 0.873). In other words, against the adsorption process, which performed only on the outer surface or large cavities (macropores) of adsorbent at low concentrations of methyl orange, the adsorption process was performed on small adsorbent pores (mesopores and micropores) at high methyl orange concentration. Based on this theory, the mean free energy of adsorption (E) was 0.029 kJ/mol, which, due to its low content (less than 8 kJ/mol), it can be said that the adsorption of methyl orange on the surface of $MgFe_2O_4$ was physical [56].

Kinetics

To investigate the mechanism of adsorption and to learn more about the adsorption process, four traditional models (pseudo-first-order, pseudo-second-order models, intraparticle diffusion, a nd Elovich) used in the adsorption process were assessed. The results are presented in Table 3 (Fig. S3). The adsorption data showed that the adsorption tradition did not follow the pseudo-first-order model. However, the pseudo-second-order model fitted very well with the experimental data and fitted perfectly with the data (R^2 = 0.9961), such that the final MO adsorption capacity on the surface of $MgFe_2O_4$ was 59.52 mg/g, which was very close to its experimental value (q_e = 56.54 mg/g).

Fittings of experimental data based on the intraparticle diffusion model showed that these data are fitted in a multi-linearity manner, and also none of the fitted lines cross the coordinate origin (Intercept is zero). The multi-linearity curves show that the more different stages of the adsorption stage (intraparticle diffusion, film layer diffusion, and interaction between adsorbate and adsorbent surface molecules) may control the rate of the absorption process [58,59]. According to Table 3, in the first stage, the value of k_{d1} (indicating the rate of absorption) is high and the amount of C_1 (showing the diffusion resistance of the film at the adsorbent surface) is low. Therefore, it can be said that in the early stages of the adsorption process, due to the high concentration of adsorbed molecules, the film diffusion resistance is low and the adsorption rate is high (the intraparticle diffusion has probably controlled the rate at this stage). In the next step, with the passage of time and the reduction of methyl orange molecules in the solution and the reduction of the driving force of the mass transfer, the film diffusion resistance increases (the large amount of C_2) and the adsorption rate will be decreased (the

Table 3. Linearized equations of kinetic models for the adsorption of MO on the $MgFe_2O_4$ surface

Kinetic Models	Linearized equations		Parameters	
Pseudo-first-order	$\ln(q_e - q_t) = \ln q_e - k_1 t$		R^2 k_1 (1/min) q_e (mg/g)	0.7014 0.063 14.695
Pseudo-second-order	$\frac{t}{q_t} = \frac{1}{k_2 q_e^2} + \frac{t}{q_e}$		R^2 k_2 (g/mg.min) q_e (mg/g)	0.9961 0.0052 59.524
Elovich	$q_t = \frac{1}{\beta}\ln(\alpha\beta) + \frac{1}{\beta}\ln t$		R^2 β (g/mg) α (mg/g.min)	0.7648 0.0998 71.707
Intraparticle diffusion	$q_t = k_d t^{0.5} + C$	Stage 1	R^2 k_{d1} (g.min$^{0.5}$/mg) C_1 (mg/g)	0.9925 14.565 -2.1668
		Stage 2	R^2 k_{d2} (g.min$^{0.5}$/mg) C_2 (mg/g)	0.9997 0.2776 53.854
Experimental data			q_e (mg/g)	56.54

q_e: the amount of MO adsorbed on the adsorbent at the equilibrium, q_t: the amount of MO adsorbed on the adsorbent at time t, k_1: the rate constant of Pseudo-first order, k_2: the rate constant of Pseudo-second order, β: the desorption constant during any one experiment, α: the initial rate of adsorption, k_d: the rate parameter of the intra-particle diffusion control stage, C: a constant related to the thickness of the boundary layer.

film diffusion controls the adsorption rate at this stage).

Inconsistency of the Elovich (R^2 = 0.7648) model with the experimental data presented that the limitation for the adsorption of dye molecules into the adsorbent surface created by the boundary layer [60].

Thermodynamics

The adsorption of MO on the adsorbent was carried out at three different temperatures to investigate the thermodynamics of the process and its results were fitted using the following linear equation, as can be seen in Fig. 8.

$$\text{Ln}\,(q_e/C_e) = (\Delta S°/R) - (\Delta H°/RT) \quad (1)$$

The fitted equation with the regression coefficient 0.908 was in good agreement with the experimental data. The values of ΔH° and ΔS° were obtained by comparing the above equation and the fitted equation (the constant amount of the gases was R = 8.314 J/mol.K). The results showed negative values for ΔH° (-46.8 kJ/mol) and ΔS° (-0.155 kJ/mol.K), so it can be concluded that the methyl orange adsorption process on the heterogeneous and magnetic surface of $MgFe_2O_4$ was exothermic. Thus, the increasing temperature would have a negative effect on the adsorption process [61].

The Gibbs free energy (ΔG°) values were also obtained -0.489, 0.236, and 2.640 kJ.mol^{-1} according to the following equation at 298, 308, and 318 K respectively [62].

$$\Delta G° = -RT\,\text{Ln}\,(q_e/C_e) \quad (2)$$

It is shown that the ΔG° is negative at 298 K (optimum temperature) indicating that the MO adsorption process on the $MgFe_2O_4$ surface is spontaneous at optimum temperature. It is also found that increasing temperature reduces the absorption driving force and the adsorption process will not spontaneously occur at higher temperatures [62]. Given the value of ΔG° (-0.489 kJ/mol^{-1}) at the optimum temperature (298 K) is between 0 and -20 that confirms the low physical interaction between

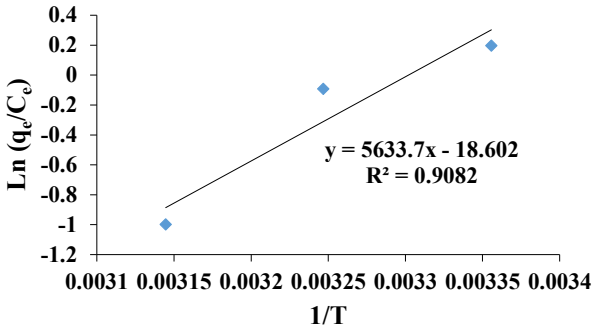

Fig. 8. Curve fitting of the thermodynamic equation for MO adsorption on the $MgFe_2O_4$ surface.

Table 4. Comparison of different nano-adsorbents for removal of dye pollutants

Nano-adsorbent	Magnetic Properties	Dye	q_{max} (mg/g)	Reference
$MgFe_2O_4$	Yes	MO	181.34	Present work
Magnetic Lignin-based Carbon Nanoparticles	Yes	MO	113	[33]
Chitosan Microspheres	No	MO	207	[57]
Organic Matters-Rich Clays	No	MO	41.67	[56]
Calcinated Organic Matters-Rich Clays	No	MO	34.48	[56]
Activated carbon/$NiFe_2O_4$	Yes	MO	182.82	[25]
CNT/λ-Fe_2O_3	Yes	MO	66.7	[55]
Hollow Molybdenum Disulfide Microspheres	No	MO	41.52	[50]
Functionalised Straw	No	MO	325.41	[30]
Co_3O_4 Nanoparticles	No	MO	46.08	[48]
Graphene Nanosheet/Fe_3O_4	Yes	MO	43.82	[1]
Zeolite/Ferrite nickel/Alginate Nanocomposite	Yes	MO	54.05	[6]

MO and the adsorbent surfaces. Moreover, it can prove by the value of ΔH° (-46.8 $kJ.mol^{-1}$) in which the adsorption of MO on the adsorbent is exothermic Physico-chemical adsorption (neither completely physical nor completely chemical) [63]. Therefore, the adsorbate can be removed from the adsorbent surface partly by heating that may be related to reversibility properties.

COMPARING THE RESULTS

Table 4 shows the properties of various adsorbents used to remove dyes from the aqueous medium. In most reported works, the maximum absorption capacity is very different from the results of the present work. In articles that used chitosan microspheres (q_m=207 mg/g) [46] and functionalized straw (q_m=325.4 mg/g) [57] as adsorbents, due to the organic nature of the adsorbents and having a high active surface, the amount of adsorption was greater than the magnetic spinel used in the present work (q_m=181.34 mg/g). The used adsorbent in the present work not only presented a suitable adsorption capacity but also showed suitable magnetic properties that it can easily separate from solution via an external magnet. So this adsorbent can be introduced as a suitable and economical adsorbent for the removal of dyes (such as methyl orange) from water.

CONCLUSIONS

In the present study, two magnetic adsorbents Fe_3O_4 (synthesized by co-precipitation method) and $MgFe_2O_4$ (synthesized by combustion method) were investigated in the methyl orange adsorption process from the aqueous solution. The results showed that the Fe_3O_4 sample had much higher magnetic strength, which could facilitate the separation of this adsorbent. This sample also had a higher surface area, which is an essential characteristic of the adsorbents. However, the use of the combustion method in the synthesis of the $MgFe_2O_4$ magnetic spinel resulted in larger pores in this sample, which could compensate for its lower surface area for the simple diffusion of large molecules of MO into the pores and be quickly absorbed. The examination of the samples in the

MO adsorption process confirmed the influence of the pore diameter on the adsorption so that the $MgFe_2O_4$ showed higher adsorption capacity than Fe_3O_4. Investigation of the adsorption isotherms and kinetics for the $MgFe_2O_4$ sample proved that the adsorption rate was not controlled by the entry of large MO molecules into the pores as well as by creating a boundary layer on the adsorbent surface. These studies showed that the adsorption step of MO on the $MgFe_2O_4$ controlled the rate of adsorption. Finally, the thermodynamic study of methyl orange adsorption on the $MgFe_2O_4$ surface revealed the process was exothermic and spontaneous. At the end of the studies, the $MgFe_2O_4$ (the maximum adsorption capacity=181.34 mg/g) sample can be suggested for the removal of dyes and water pollutants after further assessment, which will be performed in our future works.

ACKNOWLEDGMENTS

The authors gratefully acknowledge Esfarayen University of Technology [Grant Number: 93/3623] and the Research Council of Islamic Azad University, Shahr-e-Qods branch [Grant Number: 32879] for the financial support of the research.

CONFLICT OF INTEREST

There are no conflicts to declare.

REFERENCES

1. Falkenmark M, Wang-Erlandsson L, Rockström J. Understanding of water resilience in the Anthropocene. Journal of Hydrology X. 2019;2:100009.
2. Sharma VK, Feng M. Water depollution using metal-organic frameworks-catalyzed advanced oxidation processes: A review. Journal of Hazardous Materials. 2019;372:3-16.
3. Hasan M, Rashid MM, Hossain MM, Al Mesfer MK, Arshad M, Danish M, et al. Fabrication of polyaniline/activated carbon composite and its testing for methyl orange removal: Optimization, equilibrium, isotherm and kinetic study. Polymer Testing. 2019;77:105909.
4. Das TK, Ganguly S, Bhawal P, Mondal S, Das NC. A facile green synthesis of silver nanoparticle-decorated hydroxyapatite for efficient catalytic activity towards 4-nitrophenol reduction. Research on Chemical Intermediates. 2017;44(2):1189-208.
5. Tan KB, Vakili M, Horri BA, Poh PE, Abdullah AZ, Salamatinia B. Adsorption of dyes by nanomaterials: Recent developments and adsorption mechanisms. Separation and Purification Technology. 2015;150:229-42.
6. Vakili M, Rafatullah M, Salamatinia B, Abdullah AZ, Ibrahim MH, Tan KB, et al. Application of chitosan and its derivatives as adsorbents for dye removal from water and wastewater: A review. Carbohydrate Polymers. 2014;113:115-30.
7. Singh NB, Nagpal G, Agrawal S, Rachna. Water purification by using Adsorbents: A Review. Environmental Technology & Innovation. 2018;11:187-240.
8. Ibrahim RK, El-Shafie A, Hin LS, Mohd NSB, Aljumaily MM, Ibraim S, et al. A clean approach for functionalized carbon nanotubes by deep eutectic solvents and their performance in the adsorption of methyl orange from aqueous solution. Journal of Environmental Management. 2019;235:521-34.
9. Zayed AM, Abdel Wahed MSM, Mohamed EA, Sillanpää M. Insights on the role of organic matters of some Egyptian clays in methyl orange adsorption: Isotherm and kinetic studies. Applied Clay Science. 2018;166:49-60.
10. Peres EC, Slaviero JC, Cunha AM, Hosseini–Bandegharaei A, Dotto GL. Microwave synthesis of silica nanoparticles and its application for methylene blue adsorption. Journal of Environmental Chemical Engineering. 2018;6(1):649-59.
11. Bayat M, Javanbakht V, Esmaili J. Synthesis of zeolite/nickel ferrite/sodium alginate bionanocomposite via a co-precipitation technique for efficient removal of water-soluble methylene blue dye. International Journal of Biological Macromolecules. 2018;116:607-19.
12. Mehta D, Mazumdar S, Singh SK. Magnetic adsorbents for the treatment of water/wastewater—A review. Journal of Water Process Engineering. 2015;7:244-65.
13. Mahmoodi NM, Abdi J, Bastani D. Direct dyes removal using modified magnetic ferrite nanoparticle. Journal of Environmental Health Science and Engineering. 2014;12(1).
14. Kulkarni SA, Sawadh PS, Palei PK, Kokate KK. Effect of synthesis route on the structural, optical and magnetic properties of Fe3O4 nanoparticles. Ceramics International. 2014;40(1):1945-9.
15. Jiang T, Liang Y-d, He Y-j, Wang Q. Activated carbon/NiFe 2 O 4 magnetic composite: A magnetic adsorbent for the adsorption of methyl orange. Journal of Environmental Chemical Engineering. 2015;3(3):1740-51.
16. Ma Y-z, Zheng D-f, Mo Z-y, Dong R-j, Qiu X-q. Magnetic lignin-based carbon nanoparticles and the adsorption for removal of methyl orange. Colloids and Surfaces A: Physicochemical and Engineering Aspects. 2018;559:226-34.
17. Ai L, Zhang C, Chen Z. Removal of methylene blue from aqueous solution by a solvothermal-synthesized graphene/magnetite composite. Journal of Hazardous Materials. 2011;192(3):1515-24.
18. Yu F, Chen J, Chen L, Huai J, Gong W, Yuan Z, et al. Magnetic carbon nanotubes synthesis by Fenton's reagent method and their potential application for removal of azo dye from aqueous solution. Journal of Colloid and Interface Science. 2012;378(1):175-83.
19. Lu J, Jin R-N, Liu C, Wang Y-F, Ouyang X-k. Magnetic carboxylated cellulose nanocrystals as adsorbent for the removal of Pb(II) from aqueous solution. International Journal of Biological Macromolecules. 2016;93:547-56.
20. Rahmanivahid B, Pinilla-de Dios M, Haghighi M, Luque R. Mechanochemical Synthesis of CuO/MgAl2O4 and MgFe2O4 Spinels for Vanillin Production from Isoeugenol and Vanillyl Alcohol. Molecules. 2019;24(14):2597.
21. Rahmani Vahid B, Haghighi M, Toghiani J, Alaei S. Hybrid-coprecipitation vs. combustion synthesis of Mg-Al spinel based nanocatalyst for efficient biodiesel production. Energy Conversion and Management. 2018;160:220-9.
22. Kang D, Yu X, Ge M, Song W. One-step fabrication and characterization of hierarchical MgFe2O4 microspheres and their application for lead removal. Microporous and Mesoporous Materials. 2015;207:170-8.
23. Lu L, Li J, Yu J, Song P, Ng DHL. A hierarchically porous MgFe2O4/γ-Fe2O3 magnetic microspheres for efficient

removals of dye and pharmaceutical from water. Chemical Engineering Journal. 2016;283:524-34.
24. Jung K-W, Lee S, Lee YJ. Synthesis of novel magnesium ferrite (MgFe2O4)/biochar magnetic composites and its adsorption behavior for phosphate in aqueous solutions. Bioresource Technology. 2017;245:751-9.
25. Park CM, Kim YM, Kim K-H, Wang D, Su C, Yoon Y. Potential utility of graphene-based nano spinel ferrites as adsorbent and photocatalyst for removing organic/inorganic contaminants from aqueous solutions: A mini review. Chemosphere. 2019;221:392-402.
26. Reddy DHK, Yun Y-S. Spinel ferrite magnetic adsorbents: Alternative future materials for water purification? Coordination Chemistry Reviews. 2016;315:90-111.
27. Abdel Maksoud MIA, Elgarahy AM, Farrell C, Al-Muhtaseb AaH, Rooney DW, Osman AI. Insight on water remediation application using magnetic nanomaterials and biosorbents. Coordination Chemistry Reviews. 2020;403:213096.
28. Kefeni KK, Msagati TAM, Nkambule TTI, Mamba BB. Spinel ferrite nanoparticles and nanocomposites for biomedical applications and their toxicity. Materials Science and Engineering: C. 2020;107:110314.
29. Nayebzadeh H, Saghatoleslami N, Haghighi M, Tabasizadeh M. Catalytic Activity of KOH–CaO–Al2O3 Nanocomposites in Biodiesel Production: Impact of Preparation Method. International Journal of Self-Propagating High-Temperature Synthesis. 2019;28(1):18-27.
30. Neto ASB, Oliveira AC, Filho JM, Amadeo N, Dieuzeide ML, de Sousa FF, et al. Characterizations of nanostructured nickel aluminates as catalysts for conversion of glycerol: Influence of the preparation methods. Advanced Powder Technology. 2017;28(1):131-8.
31. Ma L, Chen L, Chen S. Study on the characteristics and activity of Ni–Cu–Zn ferrite for decomposition of CO2. Materials Chemistry and Physics. 2009;114(2-3):692-6.
32. Sabet Sarvestani N, Tabasizadeh M, Hossein Abbaspour-Fard M, Nayebzadeh H, Karimi-Maleh H, Chu Van T, et al. Influence of doping Mg cation in Fe3O4 lattice on its oxygen storage capacity to use as a catalyst for reducing emissions of a compression ignition engine. Fuel. 2020;272:117728.
33. Hashemzehi M, Pirouzfar V, Nayebzadeh H, Alihosseini A. Effect of synthesizing conditions on the activity of zinc-copper aluminate nanocatalyst prepared by microwave combustion method used in the esterification reaction. Fuel. 2020;263:116422.
34. Rahmani Vahid B, Haghighi M. Biodiesel production from sunflower oil over MgO/MgAl 2 O 4 nanocatalyst: Effect of fuel type on catalyst nanostructure and performance. Energy Conversion and Management. 2017;134:290-300.
35. Bhanja P, Sen T, Bhaumik A. A magnetically recoverable nanocatalyst based on functionalized mesoporous silica. Journal of Molecular Catalysis A: Chemical. 2016;415:17-26.
36. Boroujerdnia M, Obeydavi A. Synthesis and characterization of NiO/ MgAl2O4 nanocrystals with high surface area by modified sol-gel method. Microporous and Mesoporous Materials. 2016;228:289-96.
37. Amani T, Haghighi M, Rahmanivahid B. Microwave-assisted combustion design of magnetic Mg–Fe spinel for MgO-based nanocatalyst used in biodiesel production: Influence of heating-approach and fuel ratio. Journal of Industrial and Engineering Chemistry. 2019;80:43-52.
38. Zhang ZP, Rong MZ, Zhang MQ, Yuan Ce. Alkoxyamine with reduced homolysis temperature and its application in repeated autonomous self-healing of stiff polymers. Polymer Chemistry. 2013;4(17):4648.
39. Alaei S, Haghighi M, Toghiani J, Rahmani Vahid B. Magnetic and reusable MgO/MgFe 2 O 4 nanocatalyst for biodiesel production from sunflower oil: Influence of fuel ratio in combustion synthesis on catalytic properties and performance. Industrial Crops and Products. 2018;117:322-32.
40. Aruna ST, Rajam KS. Mixture of fuels approach for the solution combustion synthesis of Al2O3–ZrO2 nanocomposite. Materials Research Bulletin. 2004;39(2):157-67.
41. Granados ML, Poves MDZ, Alonso DM, Mariscal R, Galisteo FC, Moreno-Tost R, et al. Biodiesel from sunflower oil by using activated calcium oxide. Applied Catalysis B: Environmental. 2007;73(3-4):317-26.
42. Ashok A, Kennedy LJ, Vijaya JJ. Structural, optical and magnetic properties of Zn1-xMnxFe2O4 ($0 \le x \le 0.5$) spinel nano particles for transesterification of used cooking oil. Journal of Alloys and Compounds. 2019;780:816-28.
43. Zhang H, Li H, Pan H, Wang A, Souzanchi S, Xu C, et al. Magnetically recyclable acidic polymeric ionic liquids decorated with hydrophobic regulators as highly efficient and stable catalysts for biodiesel production. Applied Energy. 2018;223:416-29.
44. Li B, Cao H, Shao J, Qu M, Warner JH. Superparamagnetic Fe3O4 nanocrystals@graphene composites for energy storage devices. Journal of Materials Chemistry. 2011;21(13):5069.
45. Ge Y, Sun S, Zhou M, Chen Y, Tian Z, Zhang J, et al. Impacts of Si particle size and nitrogen pressure on combustion synthesis of Eu 2+ -doped α-SiAlON yellow phosphors. Powder Technology. 2017;305:141-6.
46. Zhai L, Bai Z, Zhu Y, Wang B, Luo W. Fabrication of chitosan microspheres for efficient adsorption of methyl orange. Chinese Journal of Chemical Engineering. 2018;26(3):657-66.
47. Mekatel EH, Amokrane S, Aid A, Nibou D, Trari M. Adsorption of methyl orange on nanoparticles of a synthetic zeolite NaA/CuO. Comptes Rendus Chimie. 2015;18(3):336-44.
48. Foo KY, Hameed BH. Factors affecting the carbon yield and adsorption capability of the mangosteen peel activated carbon prepared by microwave assisted K2CO3 activation. Chemical Engineering Journal. 2012;180:66-74.
49. Bhattacharyya K, Sharma A. Kinetics and thermodynamics of Methylene Blue adsorption on Neem () leaf powder. Dyes and Pigments. 2005;65(1):51-9.
50. Rattanapan S, Srikram J, Kongsune P. Adsorption of Methyl Orange on Coffee grounds Activated Carbon. Energy Procedia. 2017;138:949-54.
51. Halász G, Gyüre B, Jánosi IM, Szabó KG, Tél T. Vortex flow generated by a magnetic stirrer. American Journal of Physics. 2007;75(12):1092-8.
52. Yao Y, Bing H, Feifei X, Xiaofeng C. Equilibrium and kinetic studies of methyl orange adsorption on multiwalled carbon nanotubes. Chemical Engineering Journal. 2011;170(1):82-9.
53. Nassar MY, Mohamed TY, Ahmed IS, Samir I. MgO nanostructure via a sol-gel combustion synthesis method using different fuels: An efficient nano-adsorbent for the removal of some anionic textile dyes. Journal of Molecular

Liquids. 2017;225:730-40.
54. Ghaedi M, Hassanzadeh A, Kokhdan SN. Multiwalled Carbon Nanotubes as Adsorbents for the Kinetic and Equilibrium Study of the Removal of Alizarin Red S and Morin. Journal of Chemical & Engineering Data. 2011;56(5):2511-20.
55. Çelebi O, Üzüm Ç, Shahwan T, Erten HN. A radiotracer study of the adsorption behavior of aqueous Ba2+ ions on nanoparticles of zero-valent iron. Journal of Hazardous Materials. 2007;148(3):761-7.
56. Chaudhry SA, Ahmed M, Siddiqui SI, Ahmed S. Fe(III)–Sn(IV) mixed binary oxide-coated sand preparation and its use for the removal of As(III) and As(V) from water: Application of isotherm, kinetic and thermodynamics. Journal of Molecular Liquids. 2016;224:431-41.
57. Liu Q, Li Y, Chen H, Lu J, Yu G, Möslang M, et al. Superior adsorption capacity of functionalised straw adsorbent for dyes and heavy-metal ions. Journal of Hazardous Materials. 2020;382:121040.
58. Aflaki Jalali M, Dadvand Koohi A, Sheykhan M. Experimental study of the removal of copper ions using hydrogels of xanthan, 2-acrylamido-2-methyl-1-propane sulfonic acid, montmorillonite: Kinetic and equilibrium study. Carbohydrate Polymers. 2016;142:124-32.
59. Ahmadifar Z, Dadvand Koohi A. Characterization, preparation, and uses of nanomagnetic Fe3O4 impregnated onto fish scale as more efficient adsorbent for Cu2+ ion adsorption. Environmental Science and Pollution Research. 2018;25(20):19687-700.
60. Olu-Owolabi BI, Diagboya PN, Adebowale KO. Evaluation of pyrene sorption–desorption on tropical soils. Journal of Environmental Management. 2014;137:1-9.
61. Uddin MK, Baig U. Synthesis of Co3O4 nanoparticles and their performance towards methyl orange dye removal: Characterisation, adsorption and response surface methodology. Journal of Cleaner Production. 2019;211:1141-53.
62. Wu Y, Su M, Chen J, Xu Z, Tang J, Chang X, et al. Superior adsorption of methyl orange by h-MoS2 microspheres: Isotherm, kinetics, and thermodynamic studies. Dyes and Pigments. 2019;170:107591.
63. Cho E, Tahir MN, Kim H, Yu J-H, Jung S. Removal of methyl violet dye by adsorption onto N-benzyltriazole derivatized dextran. RSC Advances. 2015;5(43):34327-34.